

The Initial Mass Function of Stars: Evidence for Uniformity in Variable Systems

— SCIENCE, 4th January 2002, Vol. 295, No. 5552, p. 82–91 —

<http://www.sciencemag.org/content/>
The published paper has electronic on-line-tables only.

Pavel Kroupa

Institut für Theoretische Physik und Astrophysik, Universität Kiel
D-24098 Kiel, Germany

E-mail: pavel@astrophysik.uni-kiel.de

The distribution of stellar masses that form in one star-formation event in a given volume of space is called the initial mass function (IMF). The IMF has been estimated from low-mass brown dwarfs to very massive stars. Combining IMF estimates for different populations in which the stars can be observed individually unveils an extraordinary uniformity of the IMF. This general insight appears to hold for populations including present-day star formation in small molecular clouds, rich and dense massive star-clusters forming in giant clouds, through to ancient and metal-poor exotic stellar populations that may be dominated by dark matter. This apparent universality of the IMF is a challenge for star formation theory because elementary considerations suggest that the IMF ought to systematically vary with star-forming conditions.

The physics of star formation determines the conversion of gas to stars. The outcome of star formation are stars with a range of masses. Astrophysicists refer to the distribution of stellar masses as the stellar initial mass function. Together with the time-modulation of the star-formation rate, the IMF dictates the evolution and fate of galaxies and star clusters. The evolution of a stellar system is driven by the relative initial numbers of brown dwarfs (BDs, $\lesssim 0.072 M_{\odot}$) that do not fuse H to He, very low-mass stars ($0.072 - 0.5 M_{\odot}$), low-mass stars ($0.5 - 1 M_{\odot}$), intermediate-mass stars ($1 - 8 M_{\odot}$) and massive stars ($m > 8 M_{\odot}$). Non-luminous BDs through to dim low-mass stars remove gas from the interstellar medium (ISM), locking-up an increasing amount of the mass of galaxies over cosmological time scales. Intermediate and luminous but short-lived massive stars expel a large fraction of their mass when they die and thereby enrich the ISM with elements heavier than H and He. They heat the ISM through radiation, outflows, winds and supernovae (1, 2). It is therefore of much importance to quantify the relative numbers of stars in different mass ranges and to find systematic variations of the

IMF with different star-forming conditions. Identifying systematic variations of star formation would allow us to understand the physics involved in assembling each of the mass ranges, and thus to probe early cosmological events. Determining the IMF of a stellar population with mixed ages is a difficult problem. Stellar masses cannot be weighed directly in most instances (*I21*) so the mass has to be deduced indirectly by measuring the star’s luminosity and evolutionary state.

The history of the subject began in 1955 at the Australian National University when Edwin E. Salpeter published the first estimate (*3*) of the IMF for stars in the solar-neighborhood (*I22*). For stars with masses in the range $0.4 - 10 M_{\odot}$ he found that it can be described by a power-law form with an index $\alpha = 2.35$. This result implied a diverging mass density for $m \rightarrow 0$, which was interesting because dark matter was speculated, until the early 1990’s, to possibly be made-up of faint stars or sub-stellar objects. Studies of the stellar velocities in the solar-neighborhood also implied a large amount of missing, or dark, mass in the disk of the Milky Way (MW) (*4*). Beginning in the early 1950’s Wilhelm Gliese in Heidelberg began a careful compilation of all known stars within the solar neighborhood with accurately known distance. The edition published in 1969 became known as the famous *Gliese Catalogue of Nearby stars*, the modern version of which (*I22, 5*) constitutes the most complete and best-studied stellar sample in existence. During the early 1980’s newly developed automatic plate-measuring machines made it possible to discriminate between many distant galaxies and a few nearby main-sequence stars in the hundred thousand images on a single photographic plate. This allowed Neill Reid and Gerard Gilmore at Edinburgh Observatory to make photographic surveys of the sky with the aim of finding very low-mass stars beyond the solar neighborhood (*6*). Together with the Gliese Catalogue this survey and others that followed using the same technique significantly improved knowledge of the space density of very low-mass stars (*7, 8*). The form of the IMF for low-mass stars was further revised in the early 1990’s in Cambridge (UK) through improved theoretical understanding of the mass–luminosity relation of low mass stars and the evaluation of the observational errors due to unresolved binary systems (*9, 10*), finding confirmation by subsequent work (*11*). For massive stars John Scalo’s (*8*) determination ($\alpha \approx 2.7$) in Austin in 1986 remained in use. It is even today the most thorough analysis of the IMF in existence. It is superseded now by Phillip Massey’s (*12*) work at Tucson who demonstrated through extensive spectroscopic classification that Salpeter’s original result extends up to the most massive stars known to exist with $m \approx 120 M_{\odot}$.

Today we know that the IMF for solar-neighborhood stars flattens significantly below about $0.5 M_{\odot}$. The IMF for BDs is even shallower, as shown by Gilles Chabrier at Berkeley in 2001 (*13*), so that very-low mass stars and BDs contribute an insignificant amount to the local mass density. The need for dark matter in the MW disk also disappeared as improved kinematical data of stars in the MW disk became available (*14, 15*). Popular analytical descriptions of the IMF and some definitions are summarized in Table 1.

The Form of the IMF

Assuming all binary and higher-order stellar systems can be resolved into individual stars in some population such as the solar neighborhood (*I22*) and that only main-sequence stars are selected for, then the number of stars per pc^3 in the mass interval m to $m + dm$ is $dN = \Xi(m) dm$, where $\Xi(m)$ is the observed present-day mass function (PDMF). The number of stars per pc^3 in the absolute magnitude (*I23*) interval M_P to $M_P + dM_P$ is $dN = -\Psi(M_P) dM_P$, where $\Psi(M_P)$ is the stellar luminosity function (LF). It is constructed by counting the number of stars in the survey volume per magnitude interval, and P signifies an observational photometric

pass-band such as the V -band. Thus

$$\Xi(m) = -\Psi(M_P) (dm/dM_P)^{-1}. \quad (1)$$

Because the derivative of the stellar mass–luminosity relation (MLR), $m(M_P) = m(M_P, Z, \tau, \mathbf{s})$, is needed to calculate $\Xi(m)$, any uncertainties in stellar structure and evolution theory on the one hand or in observational ML-data on the other hand will be magnified. The dependence of the MLR on the star’s chemical composition, Z , its age, τ , and its spin vector \mathbf{s} , is explicitly stated here. This is because stars with fewer metals (lower opacity) than the Sun are brighter. Main-sequence stars brighten with time and they lose mass. Rotating stars are dimmer because of the reduced internal pressure. Mass loss and rotation also alter the MLR for intermediate and especially high-mass stars (16).

The IMF follows by correcting the observed number of main sequence stars for the number of stars that have evolved off the main sequence. Defining $t = 0$ to be the time when the Galaxy that now has an age $t = \tau_G$ formed, the number of stars per pc³ in the mass interval $m, m + dm$ that form in the time interval $t, t + dt$ is $dN = \xi(m, t) dm \times b(t) dt$. The expected time-dependence of the IMF is explicitly stated, and $b(t)$ is the time-modulation of the IMF. This is the normalized star-formation history (SFH), with $(1/\tau_G) \int_0^{\tau_G} b(t) dt = 1$. Stars that have main-sequence life-times $\tau(m) < \tau_G$ leave the stellar population unless they were born during the most recent time interval $\tau(m)$. The number density of such stars with masses in the range $m, m + dm$ still on the main sequence and the total number density of stars with $\tau(m) \geq \tau_G$, are, respectively,

$$\Xi(m) = \xi(m) \frac{1}{\tau_G} \begin{cases} \int_{\tau_G - \tau(m)}^{\tau_G} b(t) dt & , \quad \tau(m) < \tau_G, \\ \int_0^{\tau_G} b(t) dt & , \quad \tau(m) \geq \tau_G, \end{cases} \quad (2)$$

where the time-averaged IMF, $\xi(m)$, has now been defined. Thus, for low-mass stars $\Xi = \xi$, while for a sub-population of massive stars that has an age $\Delta t \ll \tau_G$, $\Xi = \xi(\Delta t/\tau_G)$ for those stars of mass m for which $\tau(m) > \Delta t$. This indicates how an observed high-mass IMF in an OB association, for example, is scaled to the Galactic-field (124) IMF for low-mass stars. In this case the different spatial distribution by different disk-scale heights of old and young stars also needs to be taken into account, which is done globally by calculating the stellar surface density in the MW disk (7, 8). In a star cluster or association with an age $\tau_{cl} \ll \tau_G$, τ_{cl} replaces τ_G in eq. 2. Examples of the time-modulation of the IMF are $b(t) = 1$ (constant star-formation rate) or a Dirac-delta function, $b(t) = \tau_{cl} \times \delta(t - t_0)$ (all stars formed at the same time t_0).

Massive stars Studying the distribution of massive stars is complicated because most of their energy is emitted at far-UV wavelengths that are not accessible from Earth, and they have short main-sequence life-times (12). For example, an $85 M_\odot$ star cannot be distinguished from a $40 M_\odot$ star on the basis of M_V alone. Constructing $\Psi(M_V)$ to get $\Xi(m)$ for a mixed-age population does not work if optical or even UV-bands are used. Instead, spectral classification and broad-band photometry for estimation of the reddening of the star-light through interstellar dust has to be performed on a star-by-star basis to measure the effective temperature, T_{eff} , and the bolometric magnitude, M_{bol} , from which m is obtained, allowing the construction of $\Xi(m)$.

Having obtained $\Xi(m)$ for a population, the IMF follows by applying eq. 2. Studies that rely on broad-band optical photometry consistently arrive at IMFs that are steeper with a power-law index $\alpha_3 \approx 3$ (see eq. 4 below), rather than $\alpha_3 = 2.2 \pm 0.1$ consistently found using spectral classification for a wide range of stellar populations (12). However, multiple systems

that are not resolved into individual stellar companions hide their less-luminous members. This is a serious problem because observations have shown that most massive stars are in binary and higher-order multiple systems (17, 18). Correcting for the missed companions leads to systematically larger $\alpha_3 \approx 2.7$ values (19). The larger value, $\alpha \approx 3 \pm 0.1$, is also suggested by a completely independent but indirect approach relying on the distribution of ultra-compact HII regions in the MW (20).

Massive main-sequence stars have substantial winds flowing outwards with velocities of a few 100 to a few 1000 km/s (21), but they do not lose more than about 10 per cent of their mass (22, 23). More problematic is that these massive stars are rapidly rotating when they form and so are sub-luminous as a result of reduced internal pressure. They decelerate during their main-sequence life-time owing to the angular-momentum loss through their winds and become more luminous more rapidly than non-rotating stars (24). The mass–luminosity relation for a population of stars that have a range of ages is therefore broadened making mass estimates from M_{bol} uncertain by up to 50 % (16), a source of error also not yet taken into account in the derivations of the IMF. Another problem is that $m \gtrsim 40 M_{\odot}$ stars may finish their assembly after burning a significant proportion of their central H so that a zero-age-main sequence may not exist for massive stars (25).

Intermediate-mass stars These stars have main-sequence life-times similar to the age of the MW disk. Solving equation 2 becomes sensitive to the SFH of the solar neighborhood and to the age and structure of the disk. None of these are known very well. Conversion of the PDMF to the IMF also depends on corrections for evolution along the main sequence if the ages of the stars were known. Deriving the IMF for intermediate-mass solar-neighborhood stars is therefore subject to difficulties that do not allow an unambiguous estimate of the IMF (26). The gap between massive and low-mass stars is bridged by assuming the IMF is continuous and differentiable.

Low-mass and very-low-mass stars in the Galactic field Galactic-field stars (124) have an average age of about 5 Ga and represent a mixture of many star-formation events. The IMF deduced for these is therefore a time-averaged IMF which is an interesting quantity for at least two reasons, namely for the mass-budget of the MW disk, and as a bench-mark against which the IMFs measured in presently occurring star-formation events can be compared with to distill possible variations about the mean.

There are two well-tried approaches to determine $\Psi(M_V)$ in eq. 1 for Galactic-field stars. The first and most straightforward method for estimating the IMF consists of creating a local volume-limited catalogue of nearby stars with accurate distance measurements. The second method is to make deep pencil-beam surveys to extract a few hundred low-mass stars from a hundred-thousand stellar and galactic images. This approach leads to larger stellar samples because many lines-of-sight into the Galactic field ranging to distances of a few 100 pc to a few kpc are possible (125). The local *nearby LF*, Ψ_{near} , and the deep *photometric LF*, Ψ_{phot} , are displayed in Fig. 1. They differ significantly for stars fainter than $M_V \approx 11.5$ causing controversy in the past (126). The solar neighborhood sample cannot have a spurious but statistically significant over-abundance of very-low-mass stars because the velocity dispersion in the disk is large, ≈ 30 pc/My. Any significant overabundance of stars within a sphere with a radius of 30 pc would disappear within one My, and cannot be created nor sustained by any physically plausible mechanism in a population of stars with stellar ages spanning the age of the MW disk.

The slope of the MLR (Fig. 2) is very small at faint luminosities leading to large uncertainties in the MF near the hydrogen burning mass limit ($\approx 0.072 M_{\odot}$, (29)). Any non-linear

structure in the MLR is mapped into observable structure in the LF (eq. 1), provided the MF does not have compensating structure. The derivative has a sharp maximum at $M_V \approx 11.5$, this being the origin of the maximum in Ψ_{phot} near $M_V = 12$ (30).

In addition to the non-linearities in the MLR relation unresolved multiple systems affect the MF derived from Ψ_{phot} . This is a serious issue because no stellar population is known to exist that has a binary proportion smaller than 50 %. Suppose an observer sees 100 systems. Of these 40, 15 and 5 are binary, triple and quadruple, respectively, these being realistic proportions. There are thus 85 companion stars which the observer is not aware of if none of the multiple systems are resolved. Because the distribution of secondary masses for a given primary mass is not uniform but typically increases with decreasing mass (31), the bias is such that low-mass stars are underrepresented in any survey that does not detect companions (32, 33, 34, 31).

Comprehensive star-count analysis of the solar neighborhood need to incorporate unresolved binary systems, metallicity and age spreads and the density fall-off perpendicular to the Galactic disk. Such studies show that the IMF can be approximated by a two-part power-law with $\alpha_1 = 1.3 \pm 0.7$, $0.08 < m/M_\odot \leq 0.5$ and $\alpha_2 = 2.2$, $0.5 < m/M_\odot \leq 1$, a result obtained for two different MLRs (35). Fig. 3 demonstrates simplified models that, however, take into account a realistic population of triple and quadruple stellar systems. The two best-fitting MLRs shown in Fig. 2 are used. The difference between the single-star and system LFs is evident in all cases, being most of the explanation of the disputed (126) discrepancy between the observed Ψ_{near} and Ψ_{phot} . It is also evident however, that the model system LFs do not approximate Ψ_{phot} very well. This is probably due to the used MLRs not accounting for the full height of the maximum in the LF.

Star clusters Most star clusters offer populations that are co-eval and equidistant with the same chemical composition. As a compensation for these advantages the extraction of faint cluster members is very arduous because of contamination from the background Galactic-field population. The first step is to obtain photometry of everything stellar in the vicinity of a cluster and to select only those stars that lie near one or a range of isochrones, taking into account that unresolved binaries are brighter than single stars. The next step is to measure proper motions and radial velocities of all candidates to select only those high-probability members that have coinciding space motion with a dispersion consistent with the a priori unknown but estimated internal kinematics of the cluster. Because nearby clusters for which proper-motion measurements are possible appear large on the sky, the observational effort is horrendous. For clusters such as globulars that are isolated the second step can be omitted, but in dense clusters stars missed due to crowding need to be corrected for. The stellar LFs in clusters turn out to have the same general shape as the photometric Galactic-field LF, Ψ_{phot} (Fig. 1), although the maximum is slightly offset depending on the metallicity of the population (30). This beautifully confirms that the maximum in the LF is due to structure in the derivative of the MLR. A 100 Ma isochrone (the age of the Pleiades) is also plotted in Fig. 2 to emphasize that for young clusters additional structure in the LF is expected (eq. 1). This is due to stars with $m < 0.6 M_\odot$ not having reached the main-sequence yet (36, 37).

LFs for star clusters are, like Ψ_{phot} , system LFs because binary systems are not resolved in the typical star-count survey. The binary-star population evolves due to encounters. After a few initial crossing times only those binary systems survive that have a binding energy larger than the typical kinetic energy of stars in the cluster. Calculations of the formation of an open star cluster demonstrate that the binary properties of stars remaining in the cluster are comparable to those in the Galactic field even if all stars initially form in binary systems (38). A further disadvantage of cluster LFs is that star clusters preferentially loose single low-mass stars across the tidal boundary as a result of ever-continuing re-distribution of energy during encounters.

With time, the retained population has an increasing binary proportion and increasing average stellar mass. The global PDMF thus flattens with time with a rate inversely proportional to the relaxation time. For highly evolved initially rich open clusters it evolves towards a delta function near the turnoff mass.

If a star cluster is younger than a few Ma classical pre-main sequence theory fails. This theory assumes hydrostatic contraction of spherical non-rotating or sometimes slowly rotating stars from idealized initial states. However, Wuchterl has shown that stars this young remember their accretion history (39). They are rotating rapidly and are non-spherical. Pre-main sequence tracks taking these effects into account are not available yet because of the severe computational difficulties. Estimates of the IMF in such very young clusters have to resort to classical calculations despite this gap in our theoretical understanding. Furthermore, the age-spread of stars is comparable to their age requiring spectroscopic classification of individual stars to place them on a theoretical (but hitherto classical) isochrone to estimate their masses (40). Binary systems are also not resolved. A few results are shown in Fig. 4. Taking the Orion nebula cluster (ONC) as the best-studied example (41, 42, 43), the figure shows how the shape of the deduced IMF varies with improving (but still classical) pre-main sequence evolution calculations. This demonstrates that any apparent sub-structure in the IMF cannot yet be relied upon to reflect possible underlying physical mechanisms of star formation.

For the much more massive and long-lived globular clusters ($N \gtrsim 10^5$ stars) theoretical stellar-dynamical work shows that the MF measured for stars near the cluster's half-mass radius is similar to the global PDMF. Inwards and outwards of this radius the MF is flatter (smaller α) and steeper (larger α), respectively. This comes from dynamical mass segregation (44). Strong mass loss in a strong tidal field flattens the global PDMF such that it no longer resembles the IMF anywhere (45).

Brown dwarfs Brown dwarfs were theoretical constructs since the early 1960's (46) until the first cases were discovered in 1995 (47). For the solar neighborhood, near-infrared large-scale surveys have now identified about 50 BDs probably closer than 25 pc. Because these objects do not have reliable distance measurements an ambiguity exists between their ages and distances. Only statistical analysis which relies on an assumed SFH for the solar neighborhood can presently constrain the IMF, finding $\alpha_0 \lesssim 1$ for the Galactic-field BD IMF (13).

Surveys of young star clusters have also discovered BDs by finding objects that extend the color-magnitude relation towards the faint locus while being kinematical members. Given the great difficulty of this endeavor only a few clusters now possess constraints on the IMF. The Pleiades star cluster has proven especially useful, given its proximity (≈ 127 pc) and young age (≈ 100 Ma). Results indicate $\alpha_0 \approx 0.5 - 0.6$ (Table 3). Estimates for other clusters (ONC, σ Ori, IC 348; Table 3) also indicate $\alpha_0 \lesssim 0.8$.

There appears to be no lower-mass limit for BDs. Free-floating planets (FFLOPs) ($\lesssim 0.01 M_\odot$) have been discovered in the very young ONC (48, 49) and in the σ Orionis cluster (50, 51, 52). The IMF for FFLOPs appears to be similar to that for the more massive BDs.

The above estimates of the IMF suffer under the same bias affecting stars, namely unseen companions. BD-BD binary systems are known to exist (47), notably in the Pleiades cluster where their offset in the color-magnitude diagram from the single-BD locus makes them conspicuous. But their frequency is not yet very well constrained because detailed scrutiny of individual objects is time-intensive on large telescopes. Calculations (38, 53) of the formation and dynamical evolution of star clusters show that after a few crossing times the binary proportion among BDs is smaller than among low-mass stars. The distribution of separations does not extend to the same distances as for stellar systems. This is a result of the weaker binding energy of BD-BD binaries. These calculations also show that after a few crossing times the

star–BD binary proportion is smaller than the star–star binary proportion. This is consistent with the results of a number of searches that have found no wide BD companions to nearby stars (47). Radial-velocity surveys of BD companions to nearby low-mass stars also show that star–BD binaries are very rare for separations $\lesssim 3$ AU. The general absence of BD companions is referred to as the *brown-dwarf desert*, because stellar companions and planets are found at such separations (54, 55). A few very wide systems with BD companions can form during the final stages of dissolution of a small cluster (56), and three such common proper-motion pairs have perhaps been found (57).

The average IMF The constraints arrived at above for $m \lesssim 1 M_{\odot}$ and $m \gtrsim 8 M_{\odot}$ can be conveniently described by a multi-part power-law form (eqs. 4 and 5 in Table 1). Because this IMF has been obtained from solar-neighborhood data for low-mass and very low-mass stars and from many clusters and OB associations for massive stars it is an average IMF. For $m < 1 M_{\odot}$ is the IMF for single stars because unseen companions are corrected for in this sample. Independent measurements of the IMF are consistent with the average multi-part power-law form (Fig. 5).

The number fractions, mass fractions and mass densities contributed to the Galactic-field total by stars in different mass-ranges are summarized in Table 2. Main-sequence stars make up about half of the baryonic matter density in the local Galactic disk. Of the stellar contribution to the matter density, BDs make up about 40 % in number and about 7 % in mass. The numbers in the table are consistent with observed star-formation events such as in Taurus–Auriga (TA). In TA groups of a few dozen stars form that do not contain stars more massive than the Sun. The table also shows that a star cluster loses about 10 % of its mass through stellar evolution within 10 My if $\alpha_3 = 2.3$ (turnoff-mass $m_{\text{to}} \approx 20 M_{\odot}$), or within 300 My if $\alpha_3 = 2.7$ (turnoff-mass $m_{\text{to}} \approx 3 M_{\odot}$). After about 10 Gy the mass loss through stellar evolution alone amounts to about 40 % if $\alpha_3 = 2.3$ or 30 % if $\alpha_3 = 2.7$. Mass loss through stellar evolution therefore poses no risk for the survival of star clusters for the IMFs discussed here, because the mass-loss rate is small enough for the cluster to adiabatically re-adjust. A star-cluster may be destroyed through mass loss from supernova explosions if $\alpha \approx 1.4$ for $8 < m/M_{\odot} \leq 120$ which would mean a mass-loss of 50 % within about 40 My when the last supernova explodes (53). None of the measurements in a resolved population has found such a low α for massive stars (Fig. 5).

Variation of the IMF and Theoretical Aspects

Is the scatter of data points in the alpha-plot (Fig. 5) a result of IMF variations? Before this can be answered affirmatively any non-physical sources for scatter in the power-law index determinations need to be assessed.

For a truly convincing departure from the average IMF a measurement would need to lie outside the conservative uncertainty range of the average IMF. Significant departures from the average IMF only occur in the shaded areas of the alpha plot. These are, however, not reliable. The upper mass range in the shaded area near $1 M_{\odot}$ poses the problem that the star-clusters have evolved such that the turn-off mass is near to this range so that conversion to masses critically depends on stellar-evolution theory and the adopted cluster ages. Some clusters such as ρ Oph are so sparse that more massive stars did not form. In both these cases the shaded range is close to the upper mass limit. This leads to possible stochastic stellar-dynamical biases because the most massive stars meet near the core of a cluster due to mass segregation, but three-body or higher-order encounters there can cause expulsions from the cluster. The shaded area near

$0.1 M_{\odot}$ poses the problem that the low-mass stars are not on the main sequence for most of the clusters studied. They are also prone to bias through mass-segregation by being underrepresented within the central cluster area that is easiest to study observationally. Especially the latter is probably biasing the M35 datum. Some effect with metallicity may be operating though, because M35 appears to have a smaller α near the H-burning mass limit than the Pleiades cluster which has a similar age but has a larger abundance of metals (Fig. 4).

Measurements of the IMF for massive stars that are too far from star-forming sites to have drifted to their positions within their life-times yield $\alpha_3 \approx 4.5$ (12). This value is discordant with the average IMF and is often quoted to be a good example of evidence for a varying IMF, being the result of isolated high-mass star-formation in small clouds. However, accurate proper-motion measurements show that even the firmest members of this isolated population have very high space motions (58). Such high velocities are most probably the result of energetic stellar-dynamical ejections when massive binary systems interact in the cores of star-clusters in normal but intense star-forming regions located in the MW disk. The large α_3 then probably comes about because the typical ejection velocity is a decreasing function of ejected stellar mass, but detailed theoretical verification is not yet available.

To address such stellar-dynamical biases an extensive theoretical library of binary-rich star clusters has been assembled (53) covering 150 My of stellar-dynamical evolution taking into account stellar evolution and assuming the average IMF in all cases. Evaluating the MF within and outside of the clusters, at different times and for clusters containing initially $800 - 10^4$ stars leads to a theoretical alpha-plot which reproduces the spread in $\alpha(lm)$ values evident in the empirical alpha-plot (Fig. 5). This verifies the conservative uncertainties adopted in the average IMF but implies that the scatter in the empirical alpha-plot around the average IMF cannot be interpreted as true variations.

Enough IMF data have been compiled to attempt the first analysis of the distribution of power-law indices. If all stellar populations have the same IMF then this should be reflected by this distribution. It ought to be a Gaussian with a mean $\langle\alpha\rangle$ value corresponding to the true IMF, and a dispersion reflecting the measurement uncertainties. The distribution of α data for $m > 2.5 M_{\odot}$ (Fig. 6) shows a narrow peak positioned at the Salpeter value, with symmetric broad wings. The empirical data are therefore not distributed like a single Gaussian function. The theoretical alpha-plot shows a distribution consistent with a single Gaussian. Its width is comparable to the broad wings in the empirical data. Interestingly, the spread, $\sigma_{\alpha,f} = 0.08$, of the narrow peak in the empirical data is very similar to the uncertainties quoted by Massey in an extensive observational determination of the IMF for massive stars, $\alpha = 2.2 \pm 0.1$. It is not clear at this stage if the empirical distribution does reflect true IMF variations. The symmetry of the broad wings suggests a superposition of at least two Gaussians with different measurement uncertainties but the same underlying IMF for massive stars.

If $\alpha_3 = 2.3 \pm 0.1$ is adopted for massive stars, then the measurement $\alpha = 1.6 \pm 0.1$ for the massive Arches cluster (Table 3), which is situated near the Galactic center and difficult to observe, would definitely mean an IMF that is top-heavy for this extreme population. There are also indications of top-heavy IMFs in star clusters in the starburst (127) galaxy M82 which has a low metallicity. The galaxy is too distant for its clusters to be resolved into individual stars and binaries, so that the stellar LF cannot be measured. However, spectroscopy of the massive M82-F cluster allows measurement of the velocity dispersion of the stars in the cluster. Together with the cluster size this gives a mass for the cluster if it is assumed that the cluster is in gravitational equilibrium. The derived mass-to-light ratio is significantly smaller than the ratio expected from the average IMF for such a young (about 60 Ma) population. The implication is that the M82-F population is significantly depleted in low-mass stars, or top-heavy (59). Stellar-dynamical modeling of forming star clusters is needed to investigate if M82-F may have

been stripped off its low-mass stars by the tidal field. Furthermore, X-ray observations of M82 suggest that the relative abundances of some heavy elements seem to be inconsistent with the expectation of the Salpeter IMF, and that stars with masses above $25 M_{\odot}$ seem to contribute significantly to the metal enrichment of the galaxy (60, 61). These studies are independent of the unresolved cluster issue and suggest that the slope of the IMF for massive stars is likely to be smaller than the Salpeter value, $\alpha_3 \lesssim 2$. This indirect approach, however, relies on exact knowledge of nucleosynthesis yields and the processes governing injection of enriched material back into the ISM. Additional evidence for variations of the IMF come from the central regions of very young star clusters. For example, the center of the ONC is deficient in low-mass stars (Fig. 4) although the global MF for this cluster is similar to the average IMF. The interpretation of a locally varying IMF depends on whether mass segregation in the ONC is primordial, or whether it is the result of stellar-dynamical evolution.

Two well-studied and resolved starburst clusters have $\alpha_3 \approx 2.3$ (30 Dor and NGC 3603, Table 3). These are also massive and very young clusters, but they oppose the suggestion from the Arches and M82-F clusters that starbursts may prefer top-heavy IMFs. From the ONC we know that the entire mass spectrum $0.05 \lesssim m/M_{\odot} \lesssim 60$ is present roughly following the average IMF (Fig. 4). Low-mass stars are also known to form in the much more massive 30 Dor cluster (62) although their IMF has not been measured yet due to the large distance of about 55 kpc. The available evidence is thus that low-mass stars and massive stars form together even in extreme environments without, as yet, convincing demonstration of a variation of the number ratio.

The observational study by Luhman (42) of many close-by star-forming regions using one consistent methodology finds that the IMF does not show measurable differences from low-density star-forming regions in small molecular clouds ($n = 0.2 - 1$ stars/pc³ in ρ Oph) to high-density cases in giant molecular clouds ($n = (1 - 5) \times 10^4$ stars/pc³ in the ONC). This result extends to the populations in the truly exotic ancient and metal-poor dwarf-spheroidal satellite galaxies. These are speculated to be dominated by dark matter and thus probably formed under conditions that were different from present-day events. Two such close companions to the MW have been observed (63, 64) finding the same MF as in globular clusters for $0.5 \lesssim m/M_{\odot} \lesssim 0.9$. Thus, again there are no significant differences to the average IMF. This apparent universality of the IMF is also supported by available chemical evolution models of the MW (65). The IMF for metal-poor and metal-rich populations of massive stars is the same (12). Between about $10 M_{\odot}$ and $m_{\text{u}} > 70 - 100 M_{\odot}$ the IMF is a power-law with $\alpha = 2.1 \pm 0.1$ for 13 clusters and OB associations in the MW (metallicity $Z \approx 0.02 = Z_{\odot}$, which is the Solar mass fraction of metals), $\alpha = 2.3 \pm 0.1$ for 10 clusters and OB associations in the Large Magellanic Cloud ($Z = 0.008$) and $\alpha = 2.3 \pm 0.1$ for one cluster in the Small Magellanic Cloud ($Z = 0.002$). The data imply that the mass of the most massive star, $m_{\text{max}} > 70 - 100 M_{\odot}$, is independent of Z , and only depends on the number of stars in the star-forming event. The most massive star that is present in a population is consistent with stars being sampled randomly from the IMF without an upper mass limit, m_{max} , the IMF taking on the meaning of a probability density function. This questions the concept of a fundamental maximum upper stellar mass, although unresolved multiple systems may be mistaken for very massive stars. It follows that radiation pressure on dust grains during star-assembly cannot be a physical mechanism establishing m_{max} (128).

However, there may be some IMF variation for very-low mass stars. Present-day star-forming clouds typically have somewhat higher metal-abundances ($\log_{10}(Z/Z_{\odot}) \approx [\text{Fe}/\text{H}] \approx +0.2$) compared to 6 Ga ago ($[\text{Fe}/\text{H}] \approx -0.3$) (66). This is the mean age of the population defining the average IMF. The data in the empirical alpha-plot indicate that some of the younger clusters may have a single-star IMF that is somewhat steeper than the average IMF if unresolved binary-stars are corrected for (53). Clouds with a larger $[\text{Fe}/\text{H}]$ appear to produce

relatively more very low-mass stars. This is tentatively supported by the M35 result (Fig. 4) and by the typically flatter MFs in globular clusters (45) that have $[\text{Fe}/\text{H}] \approx -1.5$. The recent finding that the old and metal-poor ($[\text{Fe}/\text{H}] \approx -0.6$) thick-disk population has a flatter IMF below $0.3 M_{\odot}$ with $\alpha \approx 0.5$ (67) also supports this assertion. If such a systematic effect is present, then for $m \lesssim 0.7 M_{\odot}$,

$$\alpha \approx 1.3 + \Delta\alpha [\text{Fe}/\text{H}], \quad (3)$$

with $\Delta\alpha \approx 0.5$. Many IMF measurements are needed to verify if such a variation exists because it is within the present uncertainty in α . As a possible counterexample, the IMF measured for spheroidal MW stars that have $[\text{Fe}/\text{H}] \approx -1.5$ does not appear to be significantly flatter than the average IMF (68), so the issue is far from being settled.

Theoretical considerations do suggest that for sufficiently small metallicity a gas cloud cannot cool efficiently causing the Jeans mass required for gravitational collapse to be larger. In particular, the first stars ought to have large masses because of this effect (69, 70). If the IMF of the first stars were similar to the average IMF then long-lived low-mass stars should exist that have no metals. However, none have been found (71), possibly implying that the IMF of the first stars was very different from the average IMF. Finding the remnants of these first stars poses a major challenge. An easier target is measuring the IMF for low-mass and very-low mass stars in metal-poor environments, such as young star-clusters in the Small Magellanic Cloud. Metallicity does play a role in the planetary-mass regime because the detected exo-planets occur mostly around stars that are more metal-rich than the Sun (72). This suggests that metal-richer environments may favor the formation of less-massive objects.

While the Jeans-mass argument should be valid as a general indication of the rough mass scale where fragmentation of a contracting gas cloud occurs, the concept breaks down when considering the stellar masses that form in star clusters. The central regions of clusters are denser, formally leading to smaller Jeans masses which is the opposite of the observed trend. Even in very young clusters massive stars tend to be located in the inner regions. More complex physics is involved. Stars may regulate their own mass by powerful outflows (73), and the coagulation of protostars probably plays a role in the densest regions where the cloud-core collapse time, τ_{coll} , is longer than the fragment collision time-scale which is the cluster crossing time, t_{cr} . The collapse of a fragment to a protostar with $\gtrsim 90\%$ of the final stellar mass takes no longer than $\tau_{\text{coll}} \approx 0.1$ My (39), so that $t_{\text{cr}} < 0.1$ My implies $M/R^3 > 10^5 M_{\odot}/\text{pc}^{-3}$. Such densities are only found in the centers of very populous embedded star clusters. This may explain why massive stars are usually centrally concentrated in very young clusters (74, 75). However, until accurate N -body computations are performed for a number of cases, the observed mass segregation in very young clusters cannot be taken as evidence for primordial mass segregation, and thus for coagulation and local IMF variations. For example, models of the ONC show that the degree of observed mass segregation can be established dynamically within about 2 My (Fig. 4) despite the embedded and much denser configuration having no initial mass segregation.

The origin of most stellar masses is indicated by recent observations of star formation in the ρ Oph cluster. In this modest proto-cluster the pre-stellar and protostar MFs are indistinguishable. Both are indistinguishable from the average IMF upon correction for binaries that presumably form in the cores (76, 77). The pre-stellar cores have sizes and densities that agree with the Jeans-instability argument for the conditions in the ρ Oph cloud. Cloud-fragmentation therefore appears to be the most-important mechanism shaping the stellar IMF for masses $0.05 \lesssim m/M_{\odot} \lesssim 3$, and the shape of the IMF is determined by the spectrum of density fluctuations in the molecular cloud. The computations of cloud fragmentation by Klessen are beginning to reproduce the initial stages of this process (78), but suggest that the emerging IMF depends on the star formation conditions. The empirical data indicate that stars freeze

out of the molecular gas much faster than the motions between the stars thereby preserving the distribution of density fluctuations in the cloud (79). The majority of stellar masses making up the average IMF thus do not appear to suffer subsequent modifications such as competitive accretion (80) or protostellar mergers. In particular, the flattening of the IMF near $0.5 M_{\odot}$ does not appear to be a result of the decay of few-body systems that eject unfinished protostellar cores (81), although this mechanism must operate in at least some cases. This notion as the dominant source of BDs is also in conflict with the apparent abundance of BDs in the ONC but the virtual absence of BDs within the TA star-forming clouds (82). The ejection process should operate in both environments. The problem with the unfinished-protostellar-core ejection scenario is that the BDs leave their parent cluster within a time shorter than the cluster crossing time thus rendering them unlikely to be seen in the cluster (83). However, the four BDs detected in far-outlying regions of TA (84) may constitute examples of ejected cores. The intriguing result from ρ Oph is consistent with the independent finding that the properties of binary systems in the Galactic field can be understood if most stars formed in modest ρ Oph-type clusters with primordial binary properties as observed in TA (85). However, the average IMF is also similar to the MF in the dense ONC (Fig. 4), implying that fragmentation of the pre-cluster cloud there must have proceeded similarly. It is not clear why the spectrum of density fluctuations in the pre-cluster cloud should have been similar under such different conditions.

In summary, the Galactic-field IMF (eq. 5 in Table 1) appears to be remarkably universal, with the exception in the sub-stellar mass regime. A weak empirical trend with metallicity is suggested for very-low mass stars: More metal-rich environments may be producing relatively more low-mass objects. For massive stars a correlation with star-forming conditions has not been found despite intense searches. The evidence for top-heavy IMFs come either from clusters that cannot be resolved or clusters that are very difficult to observe, or from entirely indirect arguments such as peculiar abundances of elements. This may mean that only in those rare starburst cases that are not easily accessible to the observer does the IMF begin to deviate towards a top-heavy form. Alternatively, maybe presently not understood biases are affecting the interpretation of such extreme systems that require indirect deductions about the IMF.

Uncertainties of the IMF arise because of the bias due to unresolved multiple systems and due to uncertainties in theoretical stellar models with rotation and theoretical models for ages younger than approximately one Ma. For massive stars the true IMF may be closer to Scalo's value $\alpha_3 \approx 2.7$ rather than the Salpeter value $\alpha_3 \approx 2.3$. This is valid for all studied populations provided they have similar binary-star properties.

The majority of stellar masses appear to be determined by the fragmentation of molecular clouds with little subsequent modifications such as ejections of unfinished cores or competitive accretion. It is unclear why this fragmentation process should lead to indistinguishable IMFs despite very different star forming conditions. There appears to be no empirical maximum stellar mass, nor an empirical minimum mass for BDs. Only for massive stars are cloud-core or protostellar interactions probably important. BDs are probably cores that lost their envelopes due to chance proximity to an O star. This hypothesis may explain their occurrence in relatively rich star clusters and their virtual absence in TA.

References and Notes

1. D. Chappell, J. Scalo, *Mon. Not. R. Astron. Soc.*, **325**, 1 (2001).
2. G. Hensler, *Astrophys. Space Science*, **265**, 397 (1999).
3. E.E. Salpeter, *Astrophys. J.*, **121**, 161 (1955).

4. J.N. Bahcall, *Astrophys. J.*, **287**, 926 (1984).
5. H. Jahreiß, R. Wielen, in *ESA SP-402: Proceedings of the Hipparcos - Venice'97 Symposium*, M.A.C. Perryman, P.L. Bernacca, Eds, **402**, 675 (1997).
6. N. Reid, G. Gilmore, 1982, *Mon. Not. R. Astron. Soc.*, **201**, 73 (1982).
7. G.E. Miller, J.M. Scalo, *Astrophys. J. Suppl.*, **41**, 513 (1979).
8. J.M. Scalo, *Fundam. Cosmic Physics*, **11**, 1 (1986).
9. P. Kroupa, C. A. Tout, G. Gilmore, *Mon. Not. R. Astron. Soc.* **244**, 76 (1990).
10. P. Kroupa, C. A. Tout, G. Gilmore, *Mon. Not. R. Astron. Soc.* **262**, 545 (1993) (KTG93).
11. A. Gould, J. N. Bahcall, C. Flynn, *Astrophys. J.*, **482**, 913 (1997).
12. P. Massey, in *The Stellar Initial Mass Function*, G. Gilmore, D. Howell, Eds, vol.142 of ASP Conference Series (Astronomical Society of the Pacific, San Francisco), p.17 (1998).
13. G. Chabrier, *Astrophys. J.* in press, astro-ph/0110024 (2001).
14. K. Kuijken, *Astrophys. J.*, **372**, 125 (1991).
15. C. Flynn, B. Fuchs, *Mon. Not. R. Astron. Soc.*, **270**, 471 (1994).
16. P. Massey, L.R. Penny, J. Vukovich, preprint (astro-ph/0110088).
17. G. Duchene, *et al.*, *Astron. Astrophys.*, **379**, 147 (2001).
18. T. Preibisch, *et al.*, *New Astron.*, **4**, 531 (1999).
19. R. Sagar, T. Richtler, *Astron. Astrophys.*, **250**, 324 (1991).
20. S. Casassus *et al.*, *Astron. Astrophys.*, **358**, 514 (2000).
21. R.-P. Kudritzki, J. Puls, *Ann. Rev. Astron. Astrophys.*, **38**, 613 (2000).
22. G. Garcia-Segura, N. Langer, M.-M. Mac Low, *Astron. Astrophys.*, **316**, 133 (1996).
23. G. Garcia-Segura, N. Langer, M.-M. Mac Low, *Astron. Astrophys.*, **305**, 229 (1996).
24. A. Maeder, G. Meynet, *Ann. Rev. Astron. Astrophys.*, **38**, 143 (2000).
25. A. Maeder, R. Behrend, *PASP*, in press (astro-ph/0109503) (2001).
26. J. Binney, W. Dehnen, G. Bertelli, *Mon. Not. R. Astron. Soc.*, **318**, 658 (2000).
27. P. Kroupa, *Astrophys. J.*, **453**, 350 (1995).
28. I. Baraffe *et al.*, *Astron. Astrophys.*, **337**, 403 (1998).
29. G. Chabrier, I. Baraffe, *Astron. Astrophys.*, **327**, 1039 (1997).

30. P. Kroupa, C.A. Tout, *Mon. Not. R. Astron. Soc.*, **287**, 402 (1997).
31. O. Malkov, H. Zinnecker, *Mon. Not. R. Astron. Soc.*, **321**, 149 (2001).
32. P. Kroupa, C. A. Tout, G. Gilmore, *Mon. Not. R. Astron. Soc.* **251**, 293 (1991).
33. J.A. Holtzman *et al.*, *Astrophys. J.*, **115**, 1946 (1998).
34. K.L. Luhman *et al.*, *Astrophys. J.*, **508**, 347 (1998).
35. P. Kroupa, in *Dynamics of Star Clusters and the Milky Way*, S. Deiters *et al.*, Eds, ASP Conference Series (Astronomical Society of the Pacific, San Francisco, 2001), in press (astro-ph/0011328).
36. A.N. Belikov, *et al.*, *Astron. Astrophys.*, **332**, 575 (1998).
37. G. Chabrier, I. Baraffe, *Ann. Rev. Astron. Astrophys.*, **38**, 337 (2000).
38. P. Kroupa, S.J. Aarseth, J. Hurley, *Mon. Not. R. Astron. Soc.*, **321**, 699 (2001).
39. G. Wuchterl, R.S. Klessen, *Astrophys. J.*, **560**, L185 (2001).
40. M.R. Meyer *et al.*, in *Protostars and Planets IV*, V. Mannings, A.P. Boss, S.S. Russell, Eds, p.121 (2000).
41. L.A. Hillenbrand, J.M. Carpenter, *Astrophys. J.*, **540**, 236 (2000) (HC00).
42. K.L. Luhman *et al.*, *Astrophys. J.*, **540**, 1016 (2000).
43. A.A. Muench, E.A. Lada, C.J. Lada, *Astrophys. J.*, **533**, 358 (2000).
44. E. Vesperini, D.C. Heggie, *Mon. Not. R. Astron. Soc.*, **289**, 898 (1997).
45. G. Piotto, M. Zoccali, *Astron. Astrophys.*, **345**, 485 (1999).
46. C. Hayashi, T. Nakano, *Progress of Theor. Phys.*, **30**, 460 (1963).
47. G. Basri, *Ann. Rev. Astron. Astrophys.*, **38**, 485 (2000).
48. P.W. Lucas, P.F. Roche, *Mon. Not. R. Astron. Soc.*, **314**, 858 (2000).
49. P.W. Lucas *et al.*, *Mon. Not. R. Astron. Soc.*, **326**, 695 (2001).
50. D. Barrado Y Navascués *et al.*, *Astrophys. J.*, **546**, 1006 (2001).
51. D. Barrado Y Navascués *et al.*, *Astron. Astrophys.*, in press (astro-ph/0108249).
52. V.J.S. Béjar *et al.*, *Astrophys. J.*, **556**, 830 (2001).
53. P. Kroupa, *Mon. Not. R. Astron. Soc.* **322**, 231 (2001).
54. J.L. Halbwachs *et al.*, *Astron. Astrophys.*, **355**, 581 (2000).
55. S.S. Vogt *et al.*, *Astrophys. J.*, submitted (astro-ph/0110378).

56. R. de La Fuente Marcos, *Astron. Astrophys.*, **333**, L27 (1998).
57. J.E. Gizis *et al.*, *Astrophys. J.*, **551**, L163 (2001).
58. M. Ramspeck, U. Heber, S. Moehler, *Astron. Astrophys.*, in press (astro-ph/0109472).
59. L.J. Smith, J.S. Gallagher III, *Mon. Not. R. Astron. Soc.*, **326**, 1027 (2001).
60. T.G. Tsuru, *et al.*, *Publ. Astron. Soc. Japan*, **49**, 619 (1997).
61. H. Umeda, K. Nomoto, *Astrophys. J.*, in press (astro-ph/0103241).
62. M. Sirianni *et al.*, *Astrophys. J.*, **533**, 203 (2000).
63. C.J. Grillmair *et al.*, *Astron. J.*, **115**, 144 (1998).
64. S. Feltzing, G. Gilmore, R.F.G. Wyse, *Astrophys. J.*, **516**, L17 (1999).
65. C. Chiappini, F. Matteucci, P. Padoan, *Astrophys. J.*, **528**, 711 (2000).
66. J. Binney, M. Merrifield, *Galactic Astronomy*, Princeton University Press (1998).
67. C. Reyl e, A.C. Robin, *Astron. Astrophys.*, **373**, 886 (2001).
68. A. Gould, C. Flynn, J. N. Bahcall, *Astrophys. J.*, **503**, 798, (1998)
69. R.B. Larson, *Mon. Not. R. Astron. Soc.*, **301**, 569 (1998).
70. V. Bromm, *et al.*, *Mon. Not. R. Astron. Soc.*, in press (astro-ph/0104271).
71. T.C. Beers, in *The First Stars*, A. Weiss, T. Abel, Eds, Springer, in press (2000).
72. N. C. Santos, G. Israelian, M. Mayor, in *Cool Stars, Stellar Systems and the Sun*, in press (astro-ph/0109018)
73. F.C. Adams, G. Laughlin, *Astrophys. J.*, **468**, 586 (1996).
74. I.A. Bonnell, M.R. Bate, H. Zinnecker, *Mon. Not. R. Astron. S.*, **298**, 93 (1998).
75. R.S. Klessen, *Astrophys. J.*, **550**, L77 (2001).
76. F. Motte, P. Andr e, R. Neri, *Astron. Astrophys.*, **336**, 150 (1998).
77. S. Bontemps *et al.*, *Astron. Astrophys.*, **372**, 173 (2001).
78. R.S. Klessen, *Astrophys. J.*, **556**, 837 (2001).
79. B.G. Elmegreen, *Astrophys. J.*, **530**, 277 (2000).
80. I.A. Bonnell, *et al.*, *Mon. Not. R. Astron. Soc.*, **324**, 573 (2001).
81. B. Reipurth, C. Clarke, *Astron. J.*, **122**, 432 (2001).
82. K.L. Luhman, *Astrophys. J.*, **544**, 1044 (2000).

83. I.A. Bonnell, *et al.*, *Mon. Not. R. Astron. Soc.*, **322**, 859 (2001).
84. E. L. Martin, *et al.*, *Astrophys. J. Letters*, in press (astro-ph/0110100)
85. P. Kroupa, *Mon. Not. R. Astron. Soc.*, **277**, 1491 (1995).
86. N. Reid, J.E. Gizis, *Astron. J.*, **113**, 2246 (1997).
87. H. Jahreiss, in *Science with Astronomical Near-Infrared Sky Surveys*, N. Epchtein *et al.*, Eds, Kluwer: Dordrecht, p.63 (1994).
88. T.J. Henry, P.A. Ianna, J.D. Kirkpatrick, H. Jahreiss, *Astron. J.*, **114**, 388 (1997).
89. X. Delfosse *et al.*, *Astron. Astrophys.*, **344**, 897 (1999).
90. J.-L. Beuzit *et al.*, *Astron. Astrophys.*, submitted (astro-ph/0106277).
91. R.S. Stobie, K. Ishida, J.A. Peacock, *Mon. Not. R. Astron. Soc.*, **238**, 709 (1989).
92. J.M. Scalo, in *Protostars and Planets*, T. Gehrelts, Ed., p.265 (1978).
93. G. Chabrier, *Astrophys. J.*, **554**, 1274 (2001).
94. V. Weidemann, in *Baryonic Dark Matter*, D. Lynden-Bell, G. Gilmore, Eds. (Kluwer Academic Publ., 1990), pp.87.
95. V. Weidemann *et al.*, *Astron. J.*, **104**, 187 (1992).
96. E. Moraux, J. Bouvier, J.R. Stauffer, *Astron. & Astrophys.*, **367**, 211 (2001).
97. N.C. Hambly *et al.*, *Mon. Not. R. Astron. Soc.*, **303**, 835 (1999).
98. J.R. Najita, G.P. Tiede, J.S. Carr, *Astrophys. J.*, **541**, 977 (2000).
99. B.-G. Park *et al.*, *Astron. J.*, **120**, 894 (2000).
100. J.W.M. Parker *et al.*, *Astron. J.*, **121**, 891 (2001).
101. B. Santiago *et al.*, *Astron. & Astrophys.*, **369**, 74 (2001).
102. F. Selman *et al.*, *Astron. & Astrophys.*, **347**, 532 (1999).
103. D.F. Figer, S.S. Kim *et al.*, *Astrophys. J.*, **525**, 750 (1999).
104. F. Eisenhauer *et al.*, *Astrophys. J.*, **498**, 278 (1998).
105. T.M. Herbst *et al.*, *Astrophys. J.*, **526**, L17 (1999).
106. M. Zoccali *et al.*, *Astrophys. J.*, **530**, 418 (2000).
107. N. Reid *et al.*, *Astrophys. J.*, **521**, 613 (1999).
108. J.M. Scalo, in *The Stellar Initial Mass Function*, G. Gilmore, D. Howell, Eds, vol.142 of ASP Conference Series (Astronomical Society of the Pacific, San Francisco, 1998), pp.201.

109. Z. Zheng *et al.*, *Astrophys. J.*, **555**, 393 (2001).
110. G. de Marchi, F. Paresce, *Astron. Astrophys.*, **304**, 202 (1995).
111. F. Paresce, G. de Marchi, M. Romaniello, *Astrophys. J.*, **440**, 216 (1995).
112. N.C. Hambly, R.F. Jameson, M.R.S. Hawkins, *Mon. Not. R. Astron. Soc.*, **253**, 1 (1991)
113. G. de Marchi, F. Paresce, *Astron. Astrophys.*, **304**, 211 (1995).
114. X. Delfosse *et al.*, *Astron. Astrophys.*, **364**, 217 (2000).
115. J. Andersen, *Astron. Astrophys. Rev.*, **3**, 91 (1991).
116. L. Siess, E. Dufour, M. Forestini, *Astron. Astrophys.*, **358**, 593 (2000).
117. G. Chabrier, I. Baraffe, *Astron. Astrophys.*, **327**, 1039 (1997).
118. L.A. Hillenbrand, *Astron. J.*, **113**, 1733 (1997).
119. I. Izotova, S. Parnovsky, Y. Izotov, *New Astron. Rev.*, **44**, 283 (2000).
120. T.E. Lutz, D.H. Kelker, *Publ. Astron. Soc. Pac.*, **85**, 573 (1973).
121. Stellar masses can be measured directly in binary systems. Unfortunately the Kepler orbits are available only for very few well-studied cases. These do not constitute a volume-limited unbiased sample.
122. The solar neighborhood is the region of the Milky Way close to the Sun. There is no definition of the exact radius of this region, and it is admissible to refer to the immediate solar neighborhood (within 5 pc), the solar neighborhood (within about 25 pc) and the extended solar neighborhood (within a few hundred pc). On the northern hemisphere virtually all very-low mass stars in the immediate neighborhood (129) and all low-mass stars in the neighborhood are known and have accurate distance measurements using trigonometric parallax. Their properties are catalogued in the Jahreiss-Gliese Catalogue of Nearby Stars (5) (available on-line under <http://www.ari.uni-heidelberg.de/aricns/>).
123. The absolute magnitude in the broad wavelength band P is $M_P \equiv -2.5 \log_{10}(L_P/L_{P,\odot}) + M_{P,0}$, where $L_P, L_{P,\odot}$ are the stellar and Solar luminosities, respectively, and $M_{P,0}$ is an empirical zero-point. The apparent magnitude $m_P = M_P + 5 \log_{10}d - 5$, where d is the distance of the star in pc.
124. Galactic field stars are not members of star clusters but orbit in the potential of the Milky Way disk. The solar-neighborhood (122) constitutes a local field sample.
125. The disadvantage of the LF created using this technique is that the distance measurements are indirect by relying on photometric parallax. The underlying principle of this technique is to estimate the luminosity of a star from the stellar type obtained from the color of the star or from spectral analysis. The apparent luminosity then gives a distance estimate. Such surveys are flux limited rather than volume limited. Pencil-beam surveys which do not pass through virtually the entire stellar disk are prone to Malmquist bias. This bias results from a spread of luminosities of stars that have the same color because of their dispersion of metallicities

and ages. Intrinsically more luminous stars enter the flux-limited sample. This biases the inferred absolute luminosities and the inferred stellar spatial densities. Malmquist bias can be corrected for (91), and is similar to the Lutz-Kelker bias (130).

126. The discrepancy evident in Fig. 1 between the nearby LF, Ψ_{near} , and the photometric LF, Ψ_{phot} , invoked a significant dispute (27, 86) as to the nature of this discrepancy. On the one hand (27) the difference is thought to be due to unseen companions in the deep but low-resolution surveys used to construct Ψ_{phot} , with the possibility that photometric calibration for very-low-mass stars may remain problematical so that the exact shape of Ψ_{phot} for $M_V \gtrsim 14$ is probably uncertain. On the other hand (86) the difference is thought to come from non-linearities in the $V - I$, M_V color-magnitude relation used for photometric parallax. Taking into account such structure it can be shown that the photometric surveys underestimate stellar space densities so that Ψ_{phot} moves closer to the extended estimate of Ψ_{near} using a sample of stars within 8 pc or further. While this is an important point, the extended Ψ_{near} is incomplete (129) and theoretical color-magnitude relations do not have the required degree of non-linearity. The observational color-magnitude data also do not conclusively suggest a feature with the required strength (28). Furthermore, Ψ_{phot} agrees almost perfectly with the LFs measured for star clusters of solar and population II metallicity (Fig. 1) so that it appears unlikely that non-linearities in the color-magnitude relation significantly affect Ψ_{phot} .

127. A starburst is a region in which star formation is ongoing with a very high rate. For a star-formation event to be classified as a starburst $> 10^6 M_{\odot}$ of stars have to be produced within about 1 My giving a star-formation rate of $> 1 M_{\odot}/\text{My}$ (119).

128. The physics of formation of massive stars is controversial (17). Radiation pressure from the growing core of a massive star should halt spherical accretion for $m \gtrsim 10 M_{\odot}$ so that massive stars should be produced through collisions of intermediate-mass protostars in dense cluster cores (74). Accretion through massive disks or with very high rates ($\gtrsim 10^{-5} M_{\odot}/\text{yr}$) may, however, overcome radiation pressure causing the formation of massive stars to remain an unsolved problem (25). Possible physics limiting the mass of the most massive stars is reviewed in (92). Very massive stars may finish their main-sequence life before the accretion process completes possibly rendering the most massive stars undetectable.

129. Very low-mass stars cannot be detected to large distances so that the nearby LF is poorly constrained. It is therefore important to increase the sample of nearby stars, but controversy exists as to the maximum distance to which the very-low-mass star census is complete. Using spectroscopic parallax it has been suggested that the local census of very-low mass stars is complete to distances of 8 pc and beyond (86). However, Malmquist bias (125) allows stars and unresolved binaries to enter such a flux-limited sample from much larger distances (35). The increase of the number of stars with distance using trigonometric distance measurements shows that the nearby sample becomes severely incomplete for distances larger than 5 pc and for $M_V > 12$ (87, 88). Recently discovered companions (89, 90) to known primaries in the distance range $5 < d < 12$ pc confirm that the extended sample is not yet complete.

130. The Lutz-Kelker bias affects volume-limited star-count surveys in a similar way as the Malmquist bias (125) affects flux-limited surveys. Distance observations have errors. Because the number of stars increases non-linearly with the distance there are more stars just outside the formal distance limit than inside. There are thus more stars with true distances

outside the limit that enter as a result of erroneous measurements than stars that are discounted from the survey because erroneous measurements place them outside although they are actually nearer than the distance limit. This results in a bias in the deduced average distances and stellar number densities (*120*).

131. I acknowledge use of the NASA Astrophysics Data System and partial support through DFG grant KR1635. I thank Lynne Hillenbrand, Xavier Delfosse and David Barrado Y Navascues for making available their data. I am very grateful to Linda Rowan, Philippe André, Gilles Chabrier, Christopher Tout, Volker Weidemann, Karsten Weidner and Günther Wuchterl for constructive comments.

general	$dN = \xi(m) dm = \xi_L(m) dlm$		
Scalo's IMF index (8)	$\xi_L(m) = (m \ln 10) \xi(m)$ $\Gamma(m) \equiv \frac{d}{dlm} (\log_{10} \xi_L(lm))$ $\Gamma = -x = 1 + \gamma = 1 - \alpha$ e.g. for power-law form:	$\xi_L = A m^\Gamma = A m^{-x}$ $\xi = A' m^\alpha = A' m^{-\gamma}$ $A' = A/\ln 10$	<i>gen</i> <i>Gam</i> <i>ind</i>
Salpeter(1955) (3)	$\xi_L(lm) = A m^\Gamma$ $A = 0.03 \text{ pc}^{-3} \log_{10}^{-1} M_\odot$; $0.4 \leq m/M_\odot \leq 10$	$\Gamma = -1.35$ ($\alpha = 2.35$)	<i>S</i>
Miller-Scalo(1979) (7) <i>thick long-dash-dotted line</i>	$\xi_L(lm) = A \exp \left[-\frac{(lm-lm_o)^2}{2\sigma_{lm}^2} \right]$ $A = 106 \text{ pc}^{-2} \log_{10}^{-1} M_\odot$; $lm_o = -1.02$; $\sigma_{lm} = 0.68$	$\Gamma(lm) = -\frac{(lm-lm_o)}{\sigma_{lm}^2} \log_{10} e$	<i>MS</i>
Larson(1998) (69) <i>thin short-dashed line</i>	$\xi_L(lm) = A m^{-1.35} \exp \left[-\frac{m_o}{m} \right]$ $A = -$; $m_o = 0.3 M_\odot$	$\Gamma(lm) = -1.35 + \frac{m_o}{m}$	<i>La</i>
Larson(1998) (69) <i>thin long-dashed line</i>	$\xi_L(lm) = A \left[1 + \frac{m}{m_o} \right]^{-1.35}$ $A = -$; $m_o = 1 M_\odot$	$\Gamma(lm) = -1.35 \left(1 + \frac{m_o}{m} \right)^{-1}$	<i>Lb</i>
Chabrier(2001) (93, 13) <i>thick short-dash-dotted line</i>	$\xi(m) = A m^{-\delta} \exp \left[-\left(\frac{m_o}{m} \right)^\beta \right]$ $A = 3.0 \text{ pc}^{-3} M_\odot^{-1}$; $m_o = 716.4 M_\odot$; $\delta = 3.3$; $\beta = 0.25$	$\Gamma(lm) = 1 - \delta + \beta \left(\frac{m_o}{m} \right)^\beta$	<i>Ch</i>

fig:apl

The multi-part power-law IMF:

$$\xi(m) = k \begin{cases} \left(\frac{m}{m_1} \right)^{-\alpha_0} & , \quad m_0 < m \leq m_1 & , \quad n = 0 \\ \left(\frac{m}{m_1} \right)^{-\alpha_1} & , \quad m_1 < m \leq m_2 & , \quad n = 1 \\ \left[\prod_{i=2}^{n \geq 2} \left(\frac{m_i}{m_{i-1}} \right)^{-\alpha_{i-1}} \right] \left(\frac{m}{m_n} \right)^{-\alpha_n} & , \quad m_n < m \leq m_{n+1} & , \quad n \geq 2 \end{cases} \quad (4)$$

The average, or Galactic-field, single-star IMF has $k = 0.877 \pm 0.045 \text{ stars}/(\text{pc}^3 M_\odot)$ for scaling to the solar neighborhood with

$$\begin{aligned} \alpha_0 &= +0.3 \pm 0.7 & , & \quad 0.01 \leq m/M_\odot < 0.08 & , \quad n = 0 \\ \alpha_1 &= +1.3 \pm 0.5 & , & \quad 0.08 \leq m/M_\odot < 0.50 & , \quad n = 1 \\ \alpha_2 &= +2.3 \pm 0.3 & , & \quad 0.5 \leq m/M_\odot < 1 & , \quad n = 2 \\ \alpha_3 &= \begin{matrix} +2.7 \pm 0.3 \\ +2.3 \pm 0.3 \end{matrix} & , & \quad 1 \leq m/M_\odot & , \quad n = 3. \end{aligned} \quad (5)$$

Table 1: Summary of different proposed analytical IMF forms. Notation: $lm \equiv \log_{10}(m/M_\odot) = \ln(m/M_\odot)/\ln 10$; dN is the number of single stars in the mass interval m to $m + dm$ and in the logarithmic-mass interval lm to $lm + dlm$. The mass-dependent IMF indices, $\alpha(m)$ (eq. *ind*), are plotted in Fig. 5 using the line-types defined here. Eq. *MS* was derived by Miller&Scalo assuming a constant star-formation rate and a Galactic disk age of 12 Ga (the uncertainty of which is indicated in the lower panel of Fig. 5). Larson (69) does not fit his forms (eqs. *La* and *Lb*) to solar-neighborhood star-count data but rather uses these to discuss general aspects of likely systematic IMF evolution; the m_o in eq. *La* and *Lb* given here are approximate eye-ball fits to the average IMF. In the multi-power-law IMF, $\alpha_3 = 2.3$ is consistent with the data (Fig. 5), but correction for unresolved binary systems increases this to $\alpha_3 = 2.7$. The uncertainties correspond to a 99 % confidence interval for $m > 0.5 M_\odot$ (Fig. 5), and to a 95 % confidence interval for $0.1 - 0.5 M_\odot$ (10). The nearby Hipparcos LF, $\Psi_{\text{near}}(\text{Hipp})$ (Fig. 1), has $\rho = (5.9 \pm 0.3) \times 10^{-3} \text{ stars}/\text{pc}^3$ in the interval $M_V = 5.5 - 7.5$ corresponding to the mass interval $m_2 = 0.891 - 0.687 M_\odot$ (35) using the KTG93 MLR (Fig. 2). $\int_{m_1}^{m_2} \xi(m) dm = \rho$ yields

mass range [M_\odot]	η_N [per cent]			η_M [per cent]			ρ^{st} [M_\odot/pc^3]	Σ^{st} [M_\odot/pc^2]
	α_3			α_3			α_3	α_3
	2.3	2.7	4.5	2.3	2.7	4.5	4.5	4.5
0.01–0.08	37	38	39	4.1	5.4	7.4	3.2×10^{-3}	1.6
0.08–0.5	48	49	50	27	35	48	2.1×10^{-2}	10
0.5–1	8.9	9.1	9.3	16	21	29	1.3×10^{-2}	6.4
1–8	5.7	4.6	2.4	32	30	15	6.5×10^{-3}	1.2
8–120	0.40	0.14	0.00	21	7.8	0.08	3.6×10^{-5}	6.5×10^{-3}
$\bar{m}/M_\odot =$	0.38	0.29	0.22				$\rho_{\text{tot}}^{\text{st}} = 0.043$	$\Sigma_{\text{tot}}^{\text{st}} = 19.6$

m_{max} [M_\odot]	$\alpha_3 = 2.3$		$\alpha_3 = 2.7$		m_{to} [M_\odot]	$\Delta M_{\text{cl}}/M_{\text{cl}}$ [per cent]	
	N_{cl}	M_{cl} [M_\odot]	N_{cl}	M_{cl} [M_\odot]		$\alpha_3 = 2.3$	$\alpha_3 = 2.7$
1	16	2.9	21	3.8	80	2.1	0.5
8	250	74	730	200	60	3.8	0.9
20	810	270	3400	970	40	6.5	1.6
40	2000	700	1.1×10^4	2300	20	12	3.5
60	3400	1200	2.2×10^4	6400	8	21	7.8
80	4900	1800	3.6×10^4	1.1×10^4	3	24	9.7
100	6500	2500	5.3×10^4	1.5×10^4	1	36	24
120	8300	3100	7.2×10^4	2.1×10^4	0.7	39	28

Table 2: The number fraction is $\eta_N = 100 \int_{m_1}^{m_2} \xi(m) dm / \int_{m_1}^{m_u} \xi(m) dm$. The mass fraction is $\eta_M = 100 \int_{m_1}^{m_2} m \xi(m) dm / M_{\text{cl}}$, $M_{\text{cl}} = \int_{m_1}^{m_u} m \xi(m) dm$. Both are in per cent for main-sequence stars in mass intervals m_1 to m_2 . The stellar contribution to the Oort limit, ρ^{st} , and to the Galactic-disk surface mass-density, $\Sigma^{\text{st}} = 2h\rho^{\text{st}}$. The above quantities assume for the lower and upper mass limits, respectively, $m_l = 0.01 M_\odot$ and $m_u = 120 M_\odot$. The Galactic-disk scale-height $h = 250$ pc for $m < 1 M_\odot$ (10) and $h = 90$ pc for $m > 1 M_\odot$ (8). Results are shown for the average IMF (eq. 5 in Table 1), for the high-mass-star IMF approximately corrected for unresolved companions ($\alpha_3 = 2.7, m > 1 M_\odot$), and for the PDMF in the solar neighborhood ($\alpha_3 = 4.5$ (8, 10)) which describes the distribution of stellar masses now populating the Galactic disk. The ISM contributes $\Sigma^{\text{ISM}} = 13 \pm 3 M_\odot/\text{pc}^2$, $\rho^{\text{ISM}} \approx 0.04 \pm 0.02 M_\odot/\text{pc}^3$ and stellar remnants contribute $\Sigma^{\text{rem}} \approx 3 M_\odot/\text{pc}^2$, $\rho^{\text{rem}} \approx 0.003 M_\odot/\text{pc}^3$ (94). BDs do not constitute a dynamically important mass component of the Galaxy, even when eq. 5 is extrapolated to $0.0 M_\odot$ giving $\rho^{\text{BD}} = 3.3 \times 10^{-3} M_\odot/\text{pc}^3$. The average stellar mass is $\bar{m} = \int_{m_l}^{m_u} m \xi(m) dm / \int_{m_l}^{m_u} \xi(m) dm$. N_{cl} is the number of stars that have to form in a star cluster so that the most massive star in the population has the mass m_{max} . The mass of this population is M_{cl} , and the condition is $\int_{m_{\text{max}}}^{\infty} \xi(m) dm = 1$ with $\int_{0.01}^{m_{\text{max}}} \xi(m) dm = N_{\text{cl}} - 1$. $\Delta M_{\text{cl}}/M_{\text{cl}}$ is the fraction of mass lost from the cluster due to stellar evolution, assuming that for $m \geq 8 M_\odot$ all neutron stars and black holes are kicked out due to an asymmetrical supernova explosion, but that white dwarfs are retained (95) and have masses $m_{\text{WD}} = 0.7 M_\odot$ for progenitor masses $1 \leq m/M_\odot < 8$ and $m_{\text{WD}} = 0.5 M_\odot$ for $0.7 \leq m/M_\odot < 1$. The evolution times for a star of mass m_{to} to reach the turn-off age are available in Fig. 5.

	α mass range [M_{\odot}]	α mass range [M_{\odot}]	α mass range [M_{\odot}]
Orion nebula cluster, ONC			
Muench <i>et al.</i> (43)	-0.35	+1.25	+2.35
<i>magenta small open circles with central dot</i>	0.02 – 0.08	0.08 – 0.80	0.80 – 63.1
<i>magenta large open circles with central dot</i>	+0.00	+1.00	+2.00
	0.02 – 0.08	0.08 – 0.40	0.4 – 63.10
Hillenbrand & Carpenter (41) (HC00)	+0.43		
<i>magenta large thick open circle with central dot</i>	0.02 – 0.15		
Luhman (42)	+0.70		
<i>magenta small thick open circle with central dot</i>	0.035 – 0.56		
Pleiades			
Moraux <i>et al.</i> (96)	+0.51 ± 0.15		
<i>green circles with central dot</i>	0.04 – 0.30		
Hambly <i>et al.</i> (97), from (50)	+0.56	+2.67	
<i>green circles with central dot</i>	0.065 – 0.60	0.6 – 10.0	
σ Ori			
Bejar <i>et al.</i> (52)	0.8 ± 0.4		
<i>green solid circle</i>	0.013 – 0.20		
M35			
Navascues <i>et al.</i> (50)	-0.88 ± 0.12	0.81 ± 0.02	2.59 ± 0.04
<i>green solid circle</i> ¹	0.08 – 0.2	0.2 – 0.8	0.8 – 6.0
IC 348			
Najita <i>et al.</i> (98) for MLR from (28)	+0.5		
<i>green solid circle</i>	0.015 – 0.22		
NGC 2264			
Park <i>et al.</i> (99)			+2.7
<i>green solid circle</i>			2.0 – 6.3
5 LMC regions			
Parker <i>et al.</i> (100)			+2.3 ± 0.2
<i>blue solid triangle</i>			5 – 60
NGC 1818 in LMC			
Santiago <i>et al.</i> (101), outer region		+2.5	
<i>blue solid triangle</i>		0.9 – 3	
NGC 1805 in LMC			
Santiago <i>et al.</i> (101), outer region		+3.4	
<i>blue solid triangle</i>		0.9 – 3	

Table 3: *continued*

	α mass range [M_{\odot}]	α mass range [M_{\odot}]	α mass range [M_{\odot}]
30 Dor* in LMC			
Selman <i>et al.</i> (102), $r > 3.6$ pc <i>cyan small open triangle</i>			$+2.37 \pm 0.08$ 3 – 120
Selman <i>et al.</i> (102), $1.1 < r/\text{pc} < 4.5$ <i>cyan small open triangle</i>			$+2.17 \pm 0.05$ 2.8 – 120
Sirianni <i>et al.</i> (62) <i>cyan large open triangle</i> ²		$+1.27 \pm 0.08$ 1.35 – 2.1	$+2.28 \pm 0.05$ 2.1 – 6.5
Arches cluster*			
Figer <i>et al.</i> (103), all radii <i>cyan large solid circle</i>			$+1.6 \pm 0.1$ 6.3 – 125
NGC 3603*			
Eisenhauer <i>et al.</i> (104) <i>cyan small solid circle</i>		$+1.73$ 1 – 30	$+2.7$ 15 – 70
Globular clusters			
Piotto & Zoccali (45) <i>yellow open triangles</i>	$+0.88 \pm 0.35$ 0.1 – 0.6	$+2.3$ 0.6 – 0.8	
Galactic bulge			
Holtzman <i>et al.</i> (33) <i>magenta filled square</i>	$+0.9$ 0.3 – 0.7	$+2.2$ 0.7 – 1.0	
Zoccali <i>et al.</i> (106) <i>magenta filled square</i>	$+1.43 \pm 0.13$ 0.15 – 0.5	$+2.0 \pm 0.23$ 0.5 – 1.0	
Solar Neighborhood (magenta dotted lines)			
Reid <i>et al.</i> (107)	$+1.5 \pm 0.5$ 0.02 – 0.08		
Herbst <i>et al.</i> (105)	$\leq +0.8$ 0.02 – 0.08		
Chabrier (93, 13)	$\leq +1$ 0.01 – 0.08	$+1$ / $+2$ 0.10 – 0.35 / 0.35 – 1.0	

Table 3: $\alpha(\langle lm \rangle)$ data obtained after 1998. The data are shown in Fig. 5 in addition to the previously available data set compiled by Scalo (108). Each α value is obtained at $\langle lm \rangle = (lm_2 - lm_1)/2$, $lm \equiv \log_{10} m$, by the respective authors by fitting a power-law MF over the logarithmic mass range given by m_1 and m_2 listed above. Some authors do not quote uncertainties on their α values. Notes: * are starburst clusters; ¹ thin green open circle emphasizes the low-mass M35 datum; ² the mass range $1.35 < m/M_{\odot} < 2.1$ may be incomplete and is emphasized by the cross through the cyan large open triangle.

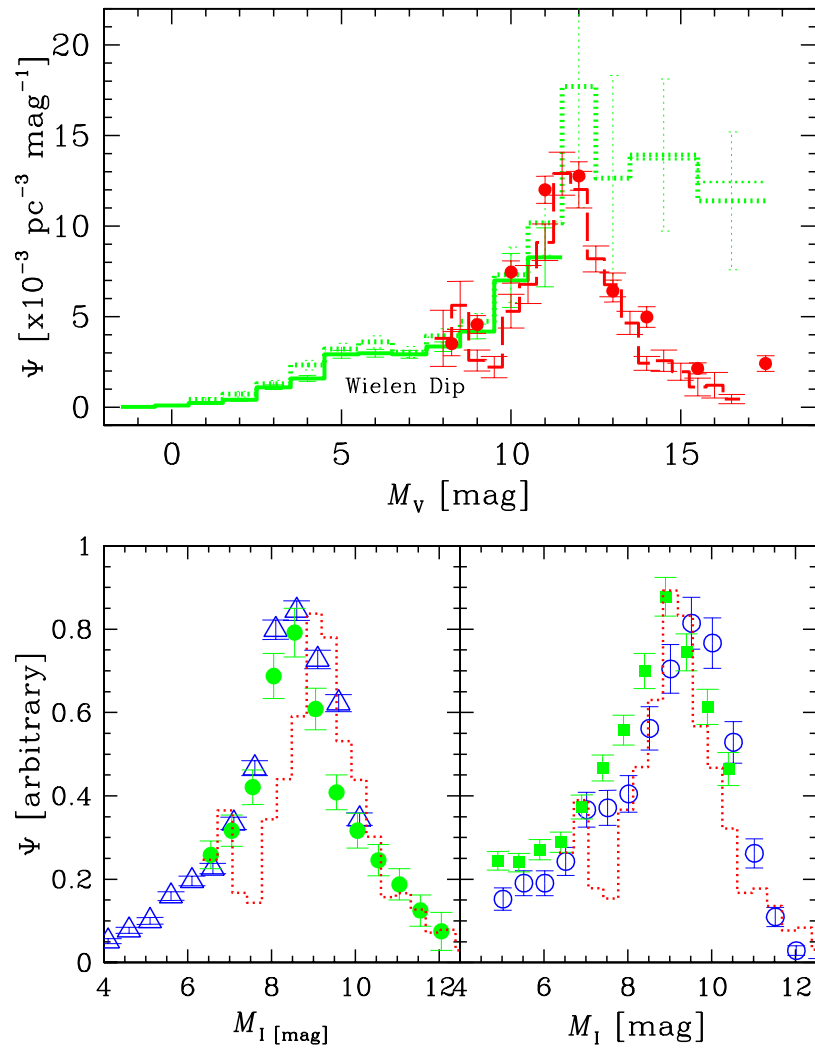


Figure 1: Next page

Fig. 1: Stellar luminosity functions (LFs, number of stars per volume element and magnitude interval) for solar-neighborhood (122) stars as a function of absolute magnitude in the V-band (upper panel) and four star clusters as a function of absolute magnitude in the I-band (lower panel). **Upper panel:** The photometric LF corrected for Malmquist bias (125) and at the midplane of the Milky Way disk (Ψ_{phot} , red histogram) is compared with the nearby LF (Ψ_{near} , green histograms) constructed from the solar neighborhood stellar sample (122). The average, ground-based $\bar{\Psi}_{\text{phot}}$ (dashed histogram, data pre-dating 1995 (27)) is confirmed by Hubble-Space-Telescope (HST) star-count data which pass through the entire Galactic disk and are thus not prone to Malmquist bias (solid circles, (109)). The ground-based volume-limited trigonometric-parallax sample (dotted histogram) systematically overestimates Ψ_{near} due to the Lutz-Kelker bias (130), thus lying above the improved estimate provided by the Hipparcos-satellite data (solid histogram, (5, 35)). The depression/plateau near $M_V = 7$ is the *Wielen dip*, named after Roland Wielen who's estimate of the LF in the 1970's for the first time unambiguously showed this feature. The thin dotted histogram at the faint end indicates the level of refinement provided by recent stellar additions (35) demonstrating that even the immediate neighborhood within 5.2 pc of the Sun probably remains incomplete at the faintest stellar luminosities. **Lower panel:** I-band LFs of stellar *systems* (single stars and unresolved binaries) in four star clusters: the globular cluster (GC) M15 (110) (distance modulus (123) $\Delta m = m - M = 15.25$ mag, blue triangles), GC NGC 6397 (111) ($\Delta m = 12.2$, green solid circles), the young open cluster Pleiades (112) ($\Delta m = 5.48$, blue open circles), and the GC 47 Tuc (113) ($\Delta m = 13.35$, green solid squares). The dotted histogram is $\bar{\Psi}_{\text{phot}}(M_I)$ from the upper panel, transformed to the I-band using the linear color-magnitude relation $M_V = 2.9 + 3.4(V - I)$ (10) and $\Psi_{\text{phot}}(M_I) = (dM_V/dM_I) \Psi_{\text{phot}}(M_V)$. The agreement in position and amplitude of the maximum in the LFs for the five different populations is impressive. This maximum results from a minimum in the derivative of the mass-luminosity relation (Fig. 2). *Note:* The figure which appeared in Science issue of 4th January 2002 has a slightly erroneous lower panel. The version shown here is corrected.

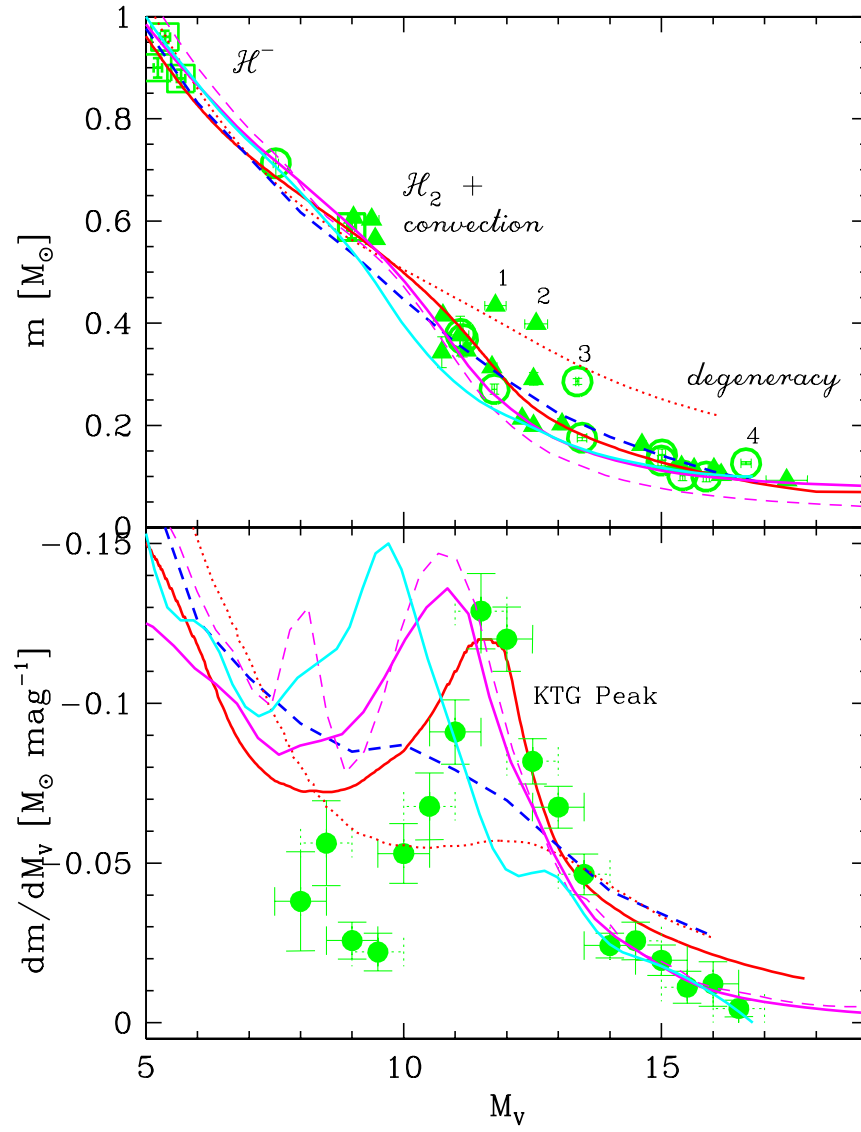


Figure 2: Next page ...

Fig. 2: The mass–luminosity relation (MLR, upper panel) is the mass of a star as a function of its absolute magnitude in the V-band. The derivative of the MLR is plotted in the lower panel. **Upper panel:** The most recent observational data (solid triangles and open circles, Delfosse et al., (114); open squares, Andersen, (115)) are compared with the empirical MLR of Scalo (blue dashed line (8)) and the semi-empirical KTG93 MLR (red solid curve (10)). The under-luminous data points 1–4 are metal-rich stars (114). The magenta solid line is a 5 Ga old isochrone and the magenta dashed line is a 0.1 Ga isochrone for solar metal abundances from Baraffe et al. (28). The cyan solid line is a 5 Ga isochrone for metallicity $Z = 0.02 Z_{\odot}$ from Siess et al. (116). As the mass of a star is reduced, H^{-} opacity becomes increasingly important through the short-lived capture of electrons by H-atoms. This results in reduced stellar luminosities for intermediate and low-mass stars. The $m(M_V)$ relation becomes less steep in the broad interval $3 < M_V < 8$ leading to the Wielen dip (Fig. 1). The $m(M_V)$ relation steepens near $M_V = 10$ because the formation of H_2 in the very outermost layers of low-mass stars increases the mean molecular weight there causing the onset of convection up to and above the photosphere. This leads to a flattening of the temperature gradient and therefore to a larger effective temperature, as opposed to an artificial case without H_2 but the same central temperature. Brighter luminosities result. Full convection establishes throughout the whole star for $m < 0.35 M_{\odot}$. The modern ML data beautifully confirm the steepening in the interval $10 < M_V < 13$ predicted in 1990 (9). The red dotted MLR demonstrates the effect of suppressing the formation of the H_2 molecule by lowering its dissociation energy from 4.48 eV to 1 eV. The $m(M_V)$ relation flattens again for $M_V > 14$, $m < 0.2 M_{\odot}$ as degeneracy in the stellar core becomes increasingly important for smaller masses limiting further contraction (46, 117). **Lower panel:** The derivatives of the same relations plotted in the upper panel are compared with $\overline{\Psi}_{\text{phot}}$ from Fig. 1 scaled to fit this figure.

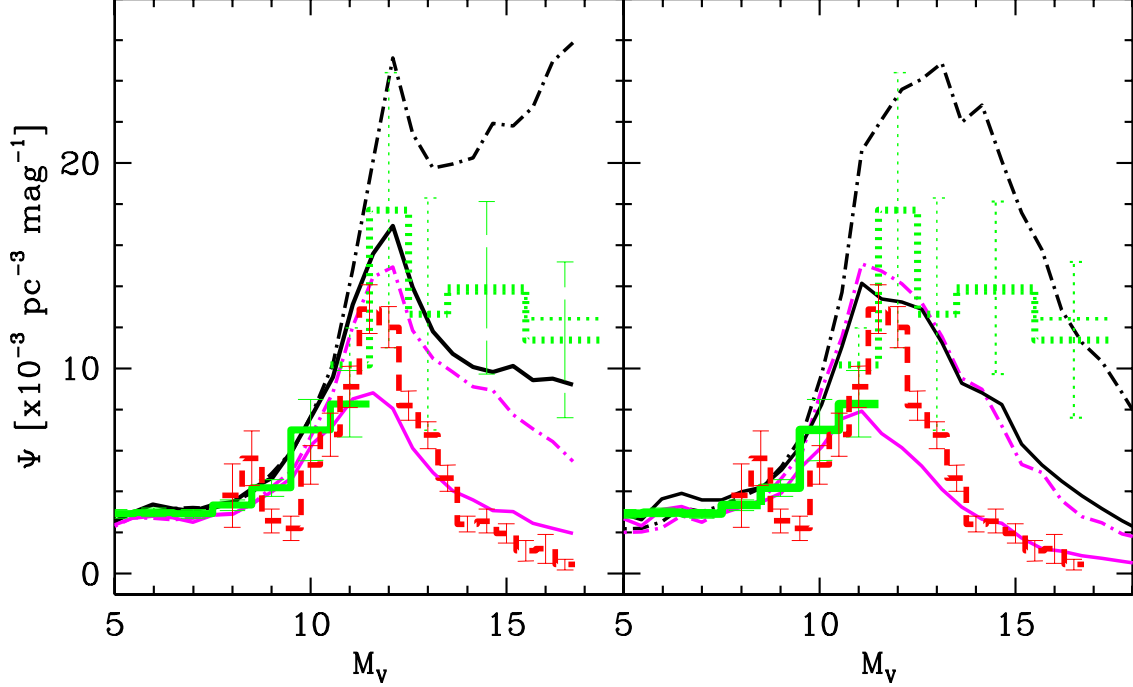


Figure 3: Model LFs (number of stars per unit volume and magnitude as a function of the absolute magnitude in the V-band) are constructed using the semi-empirical KTG93 MLR (10) (left panel) and the most advanced theoretical MLR computed by Baraffe et al. for a 5 Ga population of solar composition (28) (right panel). The MLRs are plotted in Fig. 2. The models are compared with the observed solar-neighborhood LFs shown in Fig. 1. For a given IMF, the upper (black) curves are single-star LFs. The lower curves show the unresolved system LFs in which the luminosities of stellar companions are added for a population of 8000 single stars, 8000 binaries, 3000 triples and 1000 quadruples (40:40:15:5 %, respectively). Companions with masses $0.08 \leq m/M_{\odot} \leq 1$ are combined randomly from the IMF. The models assume perfect photometry, no distance errors and no metallicity or age spread. The model system LFs thus reflect the empirical photometric LF corrected for Malmquist bias, Ψ_{phot} , whereas the observed Ψ_{near} is broadened mostly due to the metallicity and partially an age spread which is not modeled. The models are scaled to fit the LFs at $M_V \approx 7$ with equal scaling for the single-star and system LFs for a given IMF. In the left panel the IMF is a two-component power-law with Salpeter exponent $\alpha_2 = 2.3$ for $0.5 - 1.0 M_{\odot}$ but for $0.08 - 0.5 M_{\odot}$, $\alpha_1 = 1.6$ for the dot-dashed model and $\alpha_1 = 1.0$ for the solid model. In the right panel it is a one-component power-law, $\xi(m) \propto m^{-\alpha}$, over the whole mass range ($0.08 - 1 M_{\odot}$) with $\alpha = 1.8$ (dot-dashed model) and $\alpha = 1.2$ (solid model). The models are selected to roughly give similar overall deviations about the data and are not intended to be best-fit solutions. Note that the change in shape of the LF, $d^2\Psi/dM_V^2$, is an interesting observable containing information about the MLR and the underlying IMF.

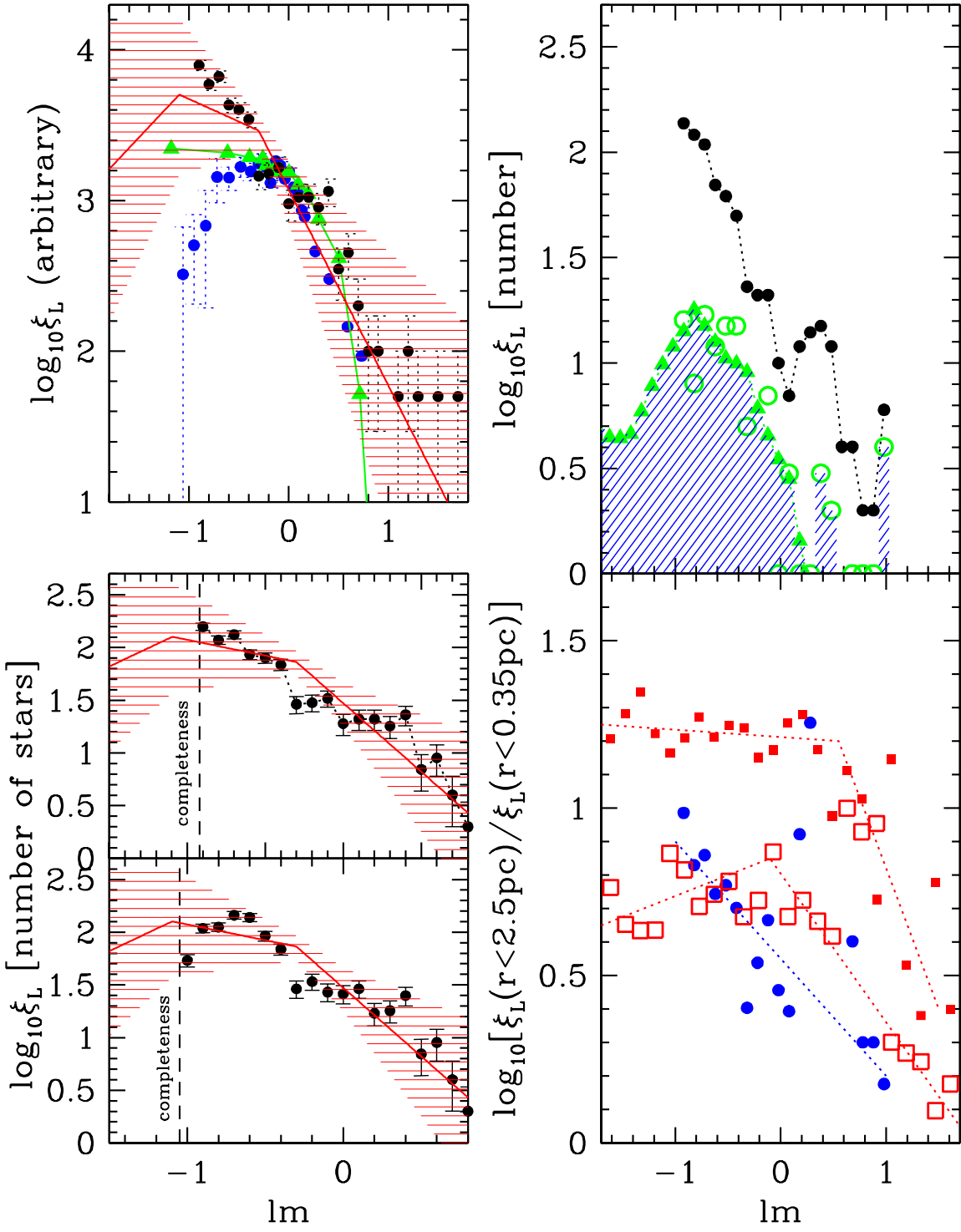


Figure 4: Next page...

Fig. 4: **Upper left panel:** The measured stellar mass functions, ξ_L , as a function of logarithmic stellar mass ($lm \equiv \log_{10}(m/M_\odot)$) in the Orion nebula cluster (ONC, solid black circles, (41)), the Pleiades (green triangles, (97)) and the cluster M35 (blue solid circles, (50)). The decrease of the M35 MF below $m \approx 0.5 M_\odot$ remains present despite using different MLRs. None of these MFs are corrected for unresolved binary systems. The average Galactic-field single-star IMF is shown as the solid red line with the associated uncertainty range (eq. 5 in Table 1). The ONC data are from the Hillenbrand optical survey within $r = 2.5$ pc of the center of the cluster. The cluster is $\tau < 2$ Ma old and has a metallicity $[\text{Fe}/\text{H}] = -0.02$. For the Pleiades, $r = 6.7$ pc, $\tau \approx 100$ Ma and $[\text{Fe}/\text{H}] = +0.01$. For M35 $r = 4.1$ pc, $\tau_{\text{cl}} \approx 160$ Ma and $[\text{Fe}/\text{H}] = -0.21$. **Lower left panel:** The shape of the ONC MF differs for very low-mass stars above the completeness limit of the survey if different pre-main sequence evolution tracks, and thus essentially different theoretical MLRs by D’Antona & Mazzitelli (DM) are employed. For more details see (41). The lower part shows the ONC MF if “DM94” pre-main sequence models are used, whereas the upper part shows the MF if “DM97/98” models are used. The average IMF is as in the upper left panel. **Upper right panel:** Mass segregation is very pronounced in the ONC. This is evident by comparing the MF for all stars within two different radial regions centered on the cluster center. The solid black circles are for all stars within $r = 2.5$ pc and the open green circles are for all stars within $r = 0.35$ pc, from the Hillenbrand ONC survey (118). The solid green triangles are for $r = 0.35$ pc, from (41). **Lower right panel:** The ratio of the MFs in the different circular survey regions of the upper right panel shows the pronounced mass segregation in the ONC. The IMF ratio, $\xi_L(r < 2.5 \text{ pc})/\xi_L(r < 0.35 \text{ pc})$, is plotted as blue solid circles. It increases with decreasing mass. This comes about because the number of low-mass stars is depleted in the inner ONC region. Stellar-dynamical models of the ONC can be used to study if the observed mass segregation (blue solid dots) can be arrived at by dynamical mass segregation. If not, then we have definite proof that the mass segregation is primordial and thus that the IMF varies at least on small scales (< 1 pc). The model snapshots shown are from model B in (38) and assume the average IMF. The masses of single stars and binary systems are counted to construct ξ_L . Initially the ratio is constant with stellar mass because the model starts with no mass segregation. The red solid squares are a snapshot at 0.9 Ma, whereas the red open squares are for 2.0 Ma. The dotted lines are eye-ball fits to the data. The data demonstrate that mass segregation develops rapidly and that by about 2 Ma the observed effect is obtained. This casts doubt on the primordial origin of the observed mass segregation.

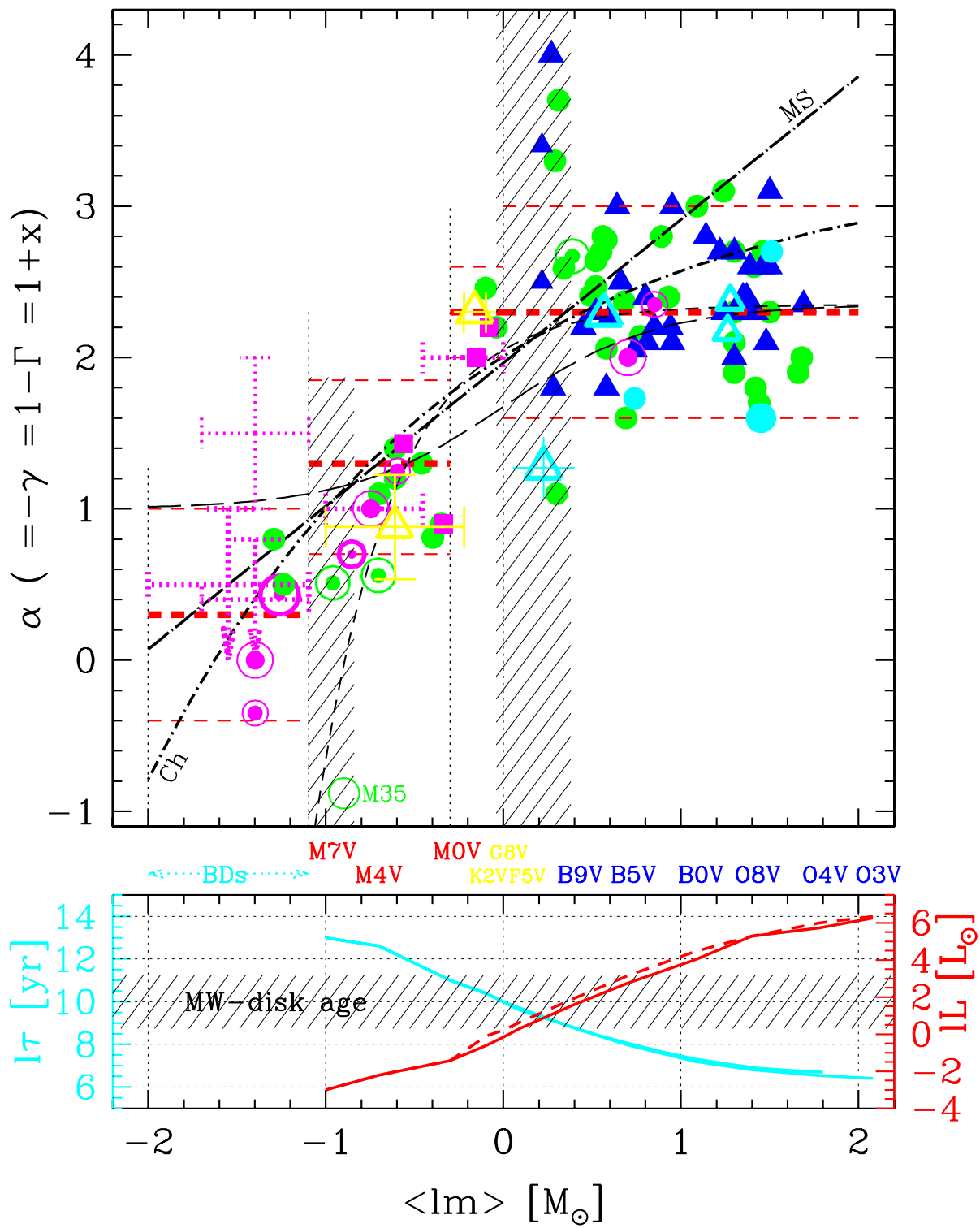


Figure 5: Next page...

Fig. 5: **Upper panel:** The alpha plot compiles measurements of the power-law index, α , as a function of the logarithmic stellar mass and so measures the shape of a MF. [Notation: $lm \equiv \log_{10}(m/M_{\odot})$, $l\tau \equiv \log_{10}(\tau/\text{yr})$, $lL \equiv \log_{10}(L/L_{\odot})$]. The shape of the MF is mapped in the upper panel by plotting measurements of α at $\langle lm \rangle = (lm_2 - lm_1)/2$ obtained by fitting power-laws, $\xi(m) \propto m^{-\alpha}$, to logarithmic mass ranges lm_1 to lm_2 (not indicated here for clarity). Many of the green circles and blue triangles are pre-1998 data compiled by Scalo (108, 53) for MW (green filled circles) and Large-Magellanic-Cloud clusters and OB associations (blue solid triangles). Newer data are also plotted using the same symbols, but some are emphasized using different symbols and colors, such as by yellow triangles for globular cluster MFs (Table 3). Unresolved multiple systems are not corrected for in all these data including the MW-bulge data. The average solar-neighborhood IMF (eq. 5 in Table 1) are the red thick short-dashed lines together with the associated uncertainty ranges. Other binary-star-corrected solar-neighborhood-IMF measurements are indicated as magenta dotted error-bars (Table 3). The quasi-diagonal black lines are analytical forms summarized in Table 1. The vertical dotted lines delineate the four mass ranges (eq. 5 in Table 1), and the shaded areas highlight those stellar mass regions where the derivation of the IMF is additionally complicated especially for Galactic field stars: for $0.08 < m/M_{\odot} < 0.15$ long pre-main sequence contraction times (37) make the conversion from an empirical LF to an IMF (eq. 1) dependent on the precise knowledge of stellar ages and the SFH. For $0.8 < m/M_{\odot} < 2.5$ uncertain main-sequence evolution, Galactic-disk age and the SFH of the MW disk do not allow accurate IMF determinations (26). **Lower panel:** The bolometric MLR, $lL(lm)$, and stellar main-sequence lifetime, $l\tau$, are plotted as a function of logarithmic stellar mass. The uncertainty in the age of the Milky-Way disk is shown as the shaded region. Stellar spectral types are written between the panels.

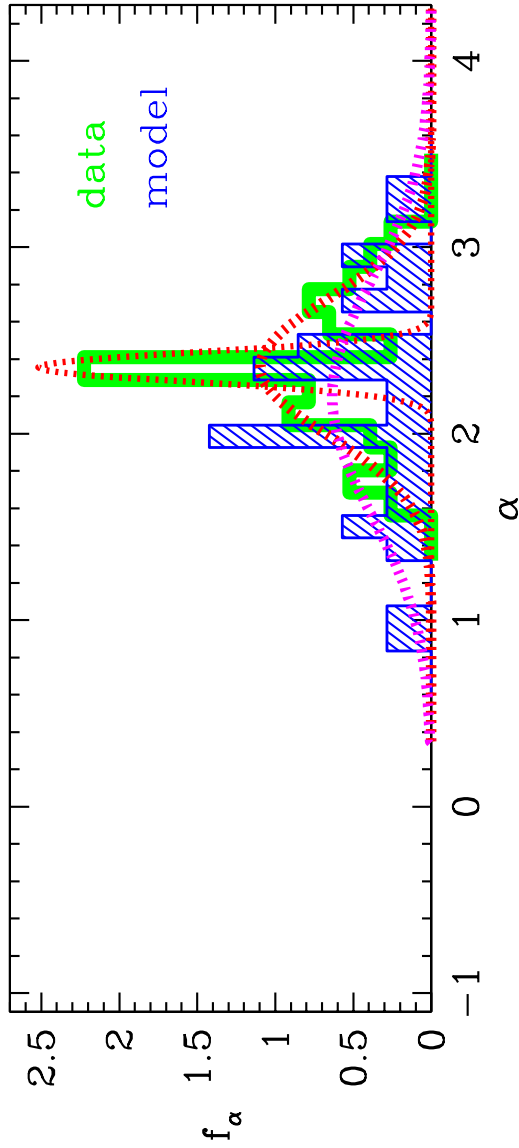


Figure 6: The histogram of MF power-law indices (α) for massive stars ($lm > 0.40$). If the α measurements are not distributed like a Gaussian function then this may imply that some of the data are different from the mean because of true IMF variations. The green histogram shows the observational data from Fig. 5. The blue shaded histogram shows theoretical values from an ensemble of 12 star clusters containing initially 800 to 10^4 stars that are snapshots at 3 and 70 Ma (53). Stellar companions in binaries are merged to give the system MFs, which are used to measure α . The assumed IMF is eq 5 in Table 1. The dotted curves are Gaussians with mean α and standard deviation, σ_α , obtained from the histograms. The theoretical data give $\langle\alpha\rangle = 2.20$, $\sigma_\alpha = 0.63$ (magenta dotted curve), and thus arrive at the input Salpeter value. The empirical data from Fig. 5 give $\langle\alpha\rangle = 2.36$, $\sigma_\alpha = 0.36$ which is the Salpeter value. Fixing $\alpha_f = \langle\alpha\rangle$ and using only $|\alpha| \leq 2\sigma_\alpha$ for the observational data gives the narrow thin red dotted Gaussian distribution which describes the Salpeter peak ($\alpha_f = 2.36$, $\sigma_{\alpha,f} = 0.08$).